NANO LETTERS

Letter

pubs.acs.org/NanoLett

Plasmonic Near-Electric Field Enhancement Effects in Ultrafast Photoelectron Emission: Correlated Spatial and Laser Polarization Microscopy Studies of Individual Ag Nanocubes

Andrej Grubisic,[†,⊥] Emilie Ringe,[‡,⊥] Claire M. Cobley,[§] Younan Xia,[§] Laurence D. Marks,[∥] Richard P. Van Duyne,*[,‡] and David J. Nesbitt*[,†]

[†]JILA, University of Colorado and National Institute of Standards and Technology, and Department of Chemistry and Biochemistry, University of Colorado, Boulder, Colorado 80309, United States

[‡]Department of Chemistry, Northwestern University, Evanston, Illinois 60208, United States

[§]Department of Biomedical Engineering, Washington University, St. Louis, Missouri 63130, United States

[∥]Department of Materials Science and Engineering, Northwestern University, Evanston, Illinois 60208, United States

Supporting Information

ABSTRACT: Electron emission from single, supported Ag nanocubes excited with ultrafast laser pulses (λ = 800 nm) is studied via spatial and polarization correlated (i) dark field scattering microscopy (DFM), (ii) scanning photoionization microscopy (SPIM), and (iii) high-resolution transmission electron microscopy (HRTEM). Laser-induced electron emission is found to peak for laser polarization aligned with cube diagonals, suggesting the critical influence of plasmonic near-field enhancement of the incident electric field on the overall electron yield. For laser pulses with photon energy below the metal work function, coherent multiphoton photoelectron emission (MPPE) is identified as the most probable mechanism responsible for electron emission from Ag nanocubes and likely metal nanoparticles/surfaces in general.

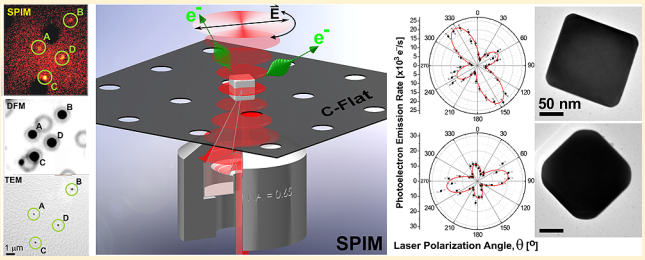

KEYWORDS: *Coherent multiphoton photoelectron emission, single-particle dark field scattering, scanning photoionization microscopy, localized surface plasmon resonance, Ag nanocubes, ultrafast excitation*

Nanotechnology research and development have become prominent subjects in the last few decades, fueled by new fundamental understanding and analytical tools. Plasmonic nanoparticles and nanostructures, in particular, have attracted much attention due to their potential application in fields ranging from medical diagnostics to optical devices and optoelectronic circuits.[1−10] The phenomenon relevant to such functionality is a localized surface plasmon resonance (LSPR): a light-induced coherent oscillation of the conduction electrons in small metallic particles. In the far-field, the localized surface plasmon manifests itself as enhanced light scattering and absorption by the particle, whereas in the near-field it generally amplifies the incident electromagnetic field ($|E_0|$) and results in increased electric field ($|E|$) near the particle surface. This local electric field enhancement is of particular interest as it increases the effective intensity of the incident electromagnetic radiation, thereby leading to phenomena such as surface enhanced Raman scattering (SERS),[11,12] improved efficiency of various nonlinear processes,[13−17] and surface enhanced fluorescence,[18] to name a few. In individual nanoparticles, near-field enhancement factors as large as $|E|/|E_0| = 10^2$ can be observed, whereas values as high as $|E|/|E_0| = 10^3$ can be attained in interparticle junctions of specially designed nanostructures.[19−21]

These large local electric field enhancements have also recently been proposed to underlie more exotic processes, such as the generation of (i) high kinetic energy (up to keV) electrons and (ii) THz radiation upon ultrafast laser illumination of metallic surfaces and metallic nanostructures, respectively.[22,23] In these cases, the observed phenomena are necessarily accompanied by electron emission—a process poorly understood for metallic nanoparticles and nanostructures irradiated with ultrafast laser pulses at a photon energy (E_{ph}) below the material work function (Φ). In particular, the exact role of the localized surface plasmon in augmenting the electron emission is presently unclear.[24−33]

Two families of mechanisms are often invoked to explain electron emission from metallic surfaces upon ultrafast excitation with sub-work function photon energies (i.e., $E_{ph} < \Phi$). In thermionic emission models,[34,35] the laser pulse momentarily heats up the conduction electrons, thus promoting a fraction of electrons in the Fermi−Dirac distribution above the metal work function, whereupon they

Received: June 16, 2012
Revised: July 17, 2012
Published: July 30, 2012

are emitted. Alternatively, the electron emission can be described in terms of a multiphoton photoelectric effect, where a particular electron is emitted after absorbing $n > \Phi/E_{ph}$ photons either simultaneously (i.e., a coherent/direct process) or sequentially (i.e., an incoherent/indirect process).[36−40] Note that another commonly encountered mechanism, that is, the field emission, is the low frequency/high intensity limit of the same electric field induced electron ejection mechanism, that of field emission, leads to multiphoton photoelectric effect in the high frequency/low intensity regime, where the current experiments operate.

The experimentally observed enhancement of electron emission from metallic nanoparticles upon resonant excitation of a plasmon can in principle be rationalized via either a thermionic or multiphoton mechanism. For example, in thermionic emission models, the plasmon could facilitate incident light absorption due to an increased particle linear absorption cross-section (σ_{ABS}), thus leading to an increased electron gas temperature, and consequently an enhancement in thermionic emissivity. On the other hand, in multiphoton photoelectron emission (MPPE) models, the build-up of coherent oscillations could lead to near-field enhancement ($|E|/|E_0|$) of the incident electric field and thus result in increased photoelectron yields.

In the current work, we have devised an experiment that distinguishes between the two possible plasmon roles, and consequently the two mechanisms, by studying electron emission from individual, supported Ag nanocubes (edge length, $d \sim 160$ nm).[41] The (i) 4-fold symmetry (nominally C_{4v} on a substrate), (ii) well-defined positioning on the substrate (i.e., face down), and (iii) relatively simple scattering spectra in the visible spectral range make nanocubes ideal for this experiment. Single Ag nanocubes exhibit two main plasmon resonances as shown in a representative dark field scattering spectrum (Figure 1): a quadrupolar mode at $\lambda \sim 480$ nm and a dipolar mode at $\lambda \sim 700$ nm. These resonances are not completely dipolar and quadrupolar, because of the symmetry-breaking presence of the substrate, as previously described, but retain a significant fractional character of the symmetric modes.[42,43] Note that other modes are also present at even higher energies.[44] However, this work focuses on the dipolar resonance, as it is the sole mode excited at 800 nm (intensity contribution >99.9% for all cubes studied).

The electron emission studies are performed in a scanning photoionization microscope (SPIM).[45,46] In this technique, schematically shown in Figure 2a, ultrafast laser pulses with center wavelength $\lambda = 800$ nm are focused by an *in vacuo* microscope objective onto a supported particle, momentarily generating high laser intensities ($I \sim 10^9$ W/cm^2) that lead to electron emission (see Supporting Information for experimental details). The two models described above predict substantially different behavior for the electron yield from Ag nanocubes as a function of the excitation laser polarization orientation in the substrate plane.

In the thermionic emission case, where the electron gas temperature is of utmost importance, the electron emission pattern upon varying laser polarization direction is expected to reflect the underlying polarization dependence of the particle's linear absorption cross-section. However, it is easily shown that any linear process (e.g., 1-photon light absorption or scattering) in structures with 3-fold rotational symmetry or higher should be independent of the laser polarization. The fundamental reason for this is that 3-fold or higher symmetry ensures that

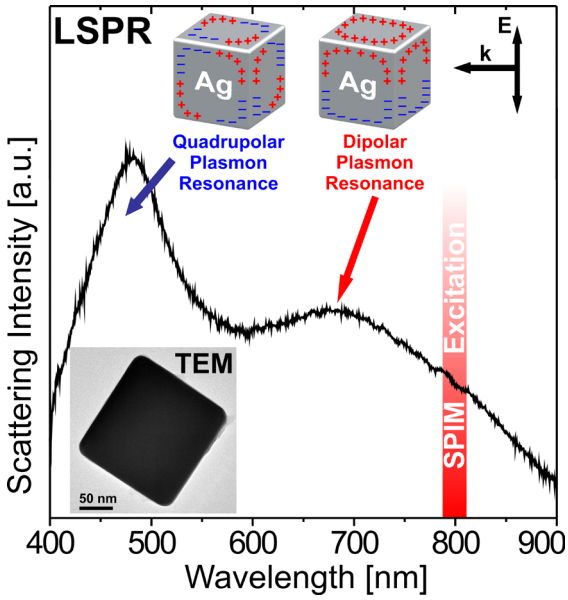

Figure 1. Dark field scattering spectrum of an individual Ag nanocube ($d \sim 160$ nm) on a C-Flat substrate. The two prominent peaks correspond to a quadrupolar ($\lambda = 480$ nm) and a dipolar ($\lambda = 690$ nm) plasmon resonance. The charge distribution for the two resonances is schematically depicted at the top of the figure for the indicated incident electromagnetic radiation. Inset: TEM image of the Ag nanocube responsible for the shown scattering spectrum.

the modes come in degenerate pairs, and thus every excited mode can be expressed as a linear combination of two (or more) degenerate modes.[47] Consequently, thermionic emission from 4-fold rotationally symmetric structures (i.e., nanocubes) would be predicted to be essentially insensitive to laser polarization (Figure 2c).

On the other hand, the multiphoton photoelectron emission rate depends on the *local* electric field component normal to the particle surface raised to the power $2n$, where n is the minimum number of photons required to overcome the material work function (i.e, $n > \Phi/E_{ph}$) and represents the order of the process. Given the Ag work function, $\Phi_{Ag} = 4.74$ eV,[48] a minimum of four ($n = 4$) photons are thus necessary for electron emission at $\lambda = 800$ nm ($E_{ph} = 1.55$ eV), implying a fourth order process. Since a plasmon enhances the local electric field, multiphoton photoelectron emission will scale roughly with $|E|/|E_0|$ to the eighth power ($I^4 \propto E^8$). Therefore, numerical electrodynamics calculations of the quantity $(|E|/|E_0|)^8$, which serves as a metric for multiphoton photoemissivity, have been performed at select excitation laser polarization orientations (Figure 2b). From the images, the corners can be clearly identified as the dominant electron sources, in agreement with previous studies that found maximum near-field enhancements at cube corners.[49−52] Most importantly, a stronger local electric field enhancement arises at the corners for the excitation polarization aligned along the cube diagonals versus perpendicular to the cube edges. This implies that multiphoton photoelectron emission will be sensitive to the laser polarization direction and resemble the four-lobe pattern shown in Figure 2c. Moreover, the laser polarization directions that result in maximum electron emission are thus expected to be aligned with the cube diagonals/corners.

dx.doi.org/10.1021/nl302271u | *Nano Lett.* 2012, 12, 4823−4829

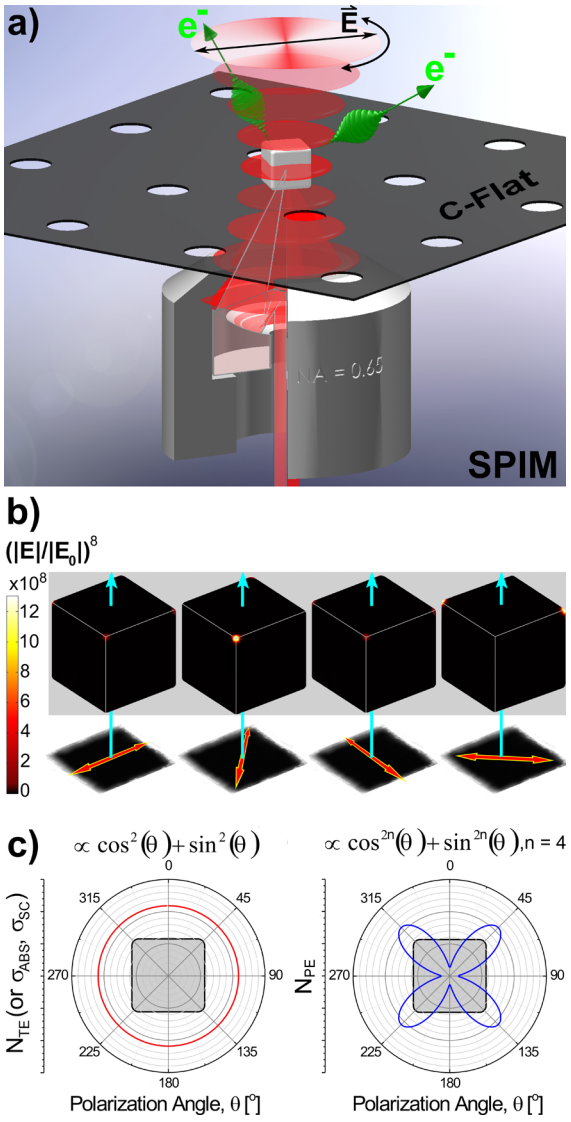

Figure 2. (a) Schematic of the scanning photoionization microscopy (SPIM) experiment. Electron emission following ultrafast laser excitation of a single Ag nanocube is monitored as a function of the laser polarization in the substrate plane. (b) COMSOL calculations for spatial distribution of the electric near-field component normal to the particle surface (2 nm outside the cube surface) for four sample orientations of the incident electric field vector. Due to the n-photon nature of the process ($n = 4$), the enhancement factor $|E|/|E_0|$ raised to the 8th (2×4) power is used as an approximate metric (see color bar) for multiphoton photoelectron emissivity. (c) Anticipated laser polarization dependence of the electron emission from individual nanocubes if dominated by a thermionic emission (N_{TE}, left) or photoelectron emission (N_{PE}, right) mechanism.

To differentiate between the two mechanisms, structural, optical, and electron emissive properties of the same single nanoparticles have been studied. Since a specific particle thus needs to be probed by a number of different experimental techniques, particle registration is essential. This is achieved by depositing the sample onto indexed, transmission electron microscope (TEM) grids and has been successfully implemented previously for correlating optical and structural properties of nanoparticles.[42] Such correlated dark field microscopy (DFM) and electron microscopy studies have greatly improved our understanding of how particle structure influences plasmonic properties in systems as varied as decahedra,[53,54] cubes,[50,51] cages,[55] spheroids,[56] and flat nanoprisms,[57,58] to name a few. In a similar fashion, we have obtained correlated SPIM, DFM, and high-resolution TEM images to study the properties of supported Ag nanocubes.

The sample data shown in Figures 3 and 4a and the Supporting Information (SI) reveal several interesting features

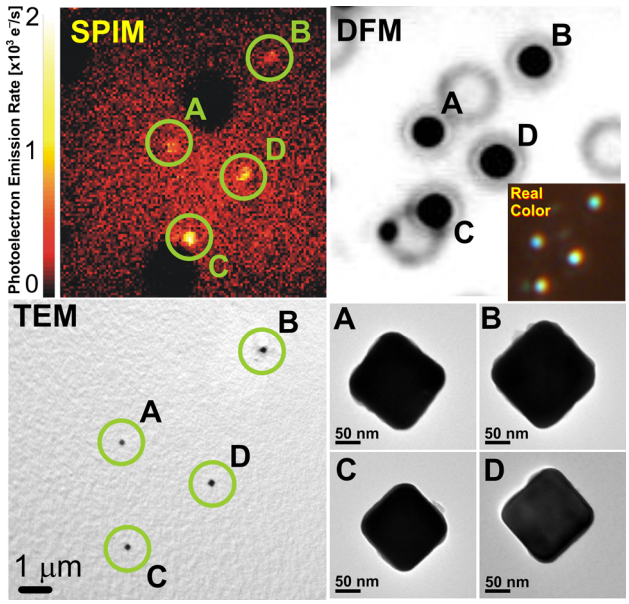

Figure 3. Spatially correlated scanning photoionization microscopy (SPIM, upper left), dark field microscopy (DFM, upper right), and transmission electron microscopy (TEM, bottom left) images of the same sample area. Magnified TEM images of the four nanocubes (labeled A–D) observed via the three different techniques are shown in the bottom right panel. Inset for the DFM image (upper right) shows the real-color image of the scattered light from the four nanocubes.

worth noting. For example, the dark field scattering signal from Ag nanocubes at $\lambda = 800$ nm exhibits no significant dependence on polarization (Figure 4a and SI), in agreement with previous observations and calculations as well as with the expectations based on the particle 4-fold rotational symmetry.[59] Slight polarization-dependent fluctuations in the scattering signal from nanocubes are observed [average $(I_{max} - I_{min})/I_{average}$ = 9%, standard deviation = 3%, $N = 20$]; however, their magnitude is substantially smaller than typically observed (>70%) in the same setup for asymmetric shapes, such as dimers and elongated structures (see SI). While the origin of these variations is presently unclear, they do not correlate with the physical orientation of the cubes (see SI), suggesting that the cause is not intrinsic to the particle structure.

In contrast to the dark field scattering signal, electron emission from Ag nanocubes is observed to strongly depend on the laser polarization, as can be seen in Figure 4a,b for the same cube. Since the electron ejection probability for any linear absorption dependent process should be insensitive to the incident laser polarization (Figure 2c), the results unambiguously rule out a thermionic emission mechanism and instead indicate that the multiphoton photoelectric effect is responsible for the observed electron emission signal. The multiphoton nature of this process is further confirmed by a power law dependence of the electron emission rate on laser intensity at λ

dx.doi.org/10.1021/nl302271u | Nano Lett. 2012, 12, 4823–4829

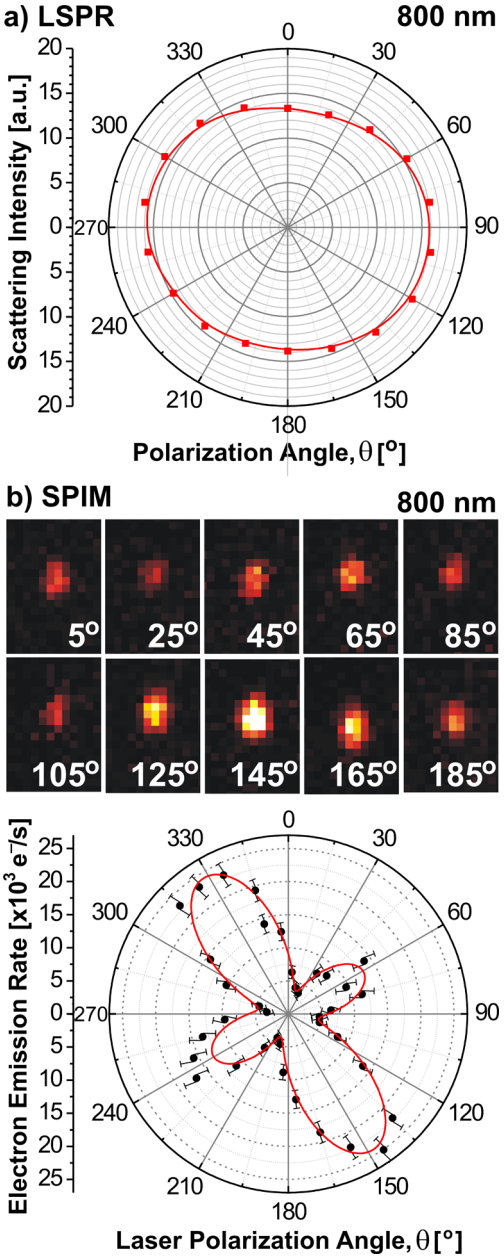

Figure 4. (a) Dark field scattering intensity from a single Ag nanocube as a function of the laser polarization angle θ (center wavelength, λ = 800 nm), revealing near isotropic behavior anticipated for a 4-fold rotational axis of symmetry. (b) A sequence of electron photoemission images (top) from the same Ag nanocube as a function of laser polarization angle, immediately signaling strongly anisotropic behavior. A polar plot (bottom) of SPIM intensity for a single Ag nanocube as a function of laser polarization angles recorded at a laser intensity $I = 4.5 \times 10^9$ W/cm^2. Note the clear four-lobed anisotropy, which for a 4-fold rotational axis of symmetry is qualitatively inconsistent with any linear absorption dependent process such as thermionic emission, but provides strong support for a coherent multiphoton photoemission model.

= 800 nm, where the expected ensemble-averaged exponent value $n = 4.0(1)$ has been measured in a sample of $N = 7$ cubes (see SI).

Since photoelectron emission is strongly influenced by the local electric field at the particle surface, the electron emission yield would be expected to peak when the laser polarization aligns with the regions of highest electric field enhancement, that is, cube corners.[43,44,49,50,52] This is precisely what has been experimentally observed in correlated SPIM-TEM measurements on $N = 10$ Ag nanocubes (Figure 5). Note that a similarly marked increase in the SERS signal (i.e., also nonlinearly dependent on local electric field enhancement) had been observed in earlier studies for laser polarization aligned with the nanocube diagonals.[52] The present finding of a

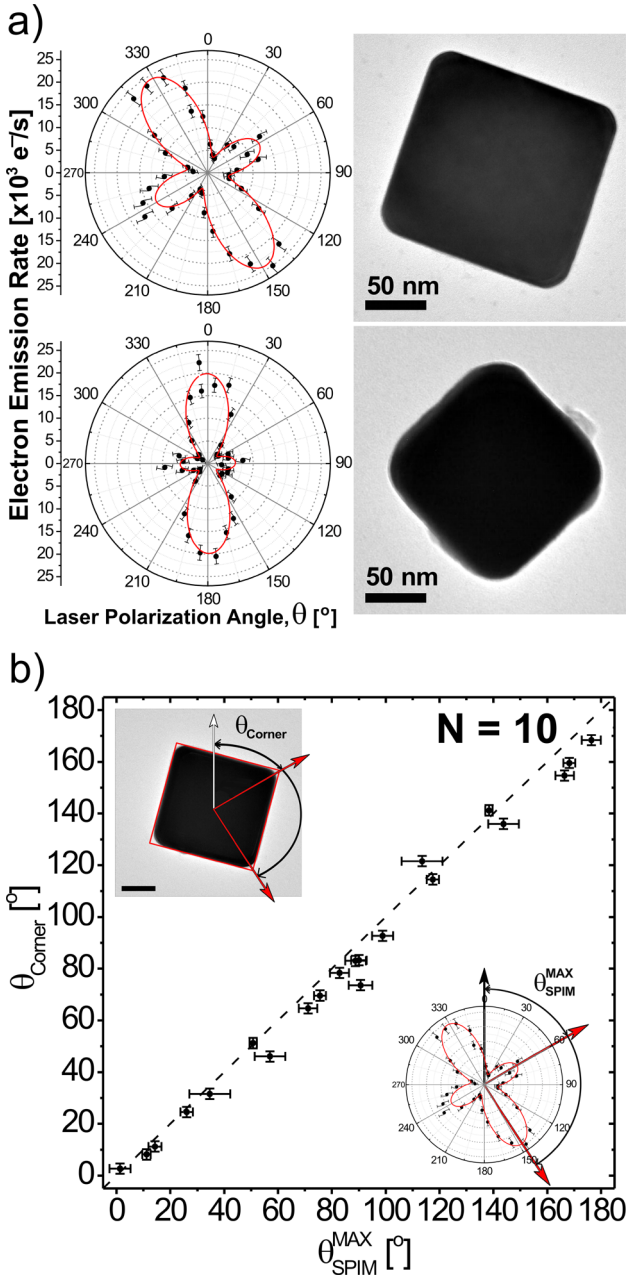

Figure 5. (a) Polar plots of electron emission rates from two supported, Ag nanocubes (upper left: $I = 4.5 \times 10^9$ W/cm^2; bottom left: $I = 5.6 \times 10^9$ W/cm^2) as a function of laser polarization orientation. Corresponding TEM images (right) of the two nanocubes in the same reference frame. Note that the peak electron emission is always observed when the laser polarization aligns with the cube face diagonals (i.e., corners). (b) Quantitative correspondence between (i) direction of the cube corners (θ_{Corner}) and (ii) laser polarization direction resulting in maximum electron emission (θ_{SPIM}^{MAX}) for a sample of $N = 10$ Ag nanocubes.

dx.doi.org/10.1021/nl302271u | Nano Lett. 2012, 12, 4823−4829

similar polarization-dependent electron ejection propensity further identifies the electric field enhancement induced by the localized surface plasmon resonance as critical for efficient electron emission.

With electron emission from plasmonic nanoparticles established as a multiphoton photoelectric process for ultrafast laser excitation with sub-work function photon energies, the question remains whether the process occurs via a *coherent*[36−38] or *incoherent*[40] absorption of multiple photons. In the latter case, population change in the intermediate states occurs, whereas an in-phase excited state is generated by the radiation field in the former case, with no accompanying change in the intermediate state populations. A general model has been recently proposed by Yalunin et al. that specifically describes coherent MPPE from a surface of a free-electron metal (i.e., perfect electric conductor) upon ultrafast excitation.[39] Since Ag acts as a relatively good free-electron metal in the relevant wavelength range,[60] their theory can be employed to compare the observed experimental photoelectron emission rates from Ag nanocubes with predictions for a coherent process. To include plasmonic excitations into their theory, we treat plasmons classically by assuming that this incident electric field can be scaled by the local plasmon-induced near-field enhancement factor, $|E|/|E_0|$. This assumption of a classical limit is justified since multiphoton photoelectron emission under our typical experimental conditions generate plasmon numbers ($N_{Pl} \sim 10^6$) orders of magnitude larger than the number ($N_{Pl} = n = 4$) energetically required for electron ejection.[29,61]

To implement this theory further, typical electric field enhancement factors of $|E|/|E_0| \sim 12$ have been calculated using COMSOL at the corners of a representative cube in vacuum (edge length, $d = 160$ nm; corner roundness, $r = 8$ nm) for $\lambda = 800$ nm excitation. This value is in qualitative agreement with previously reported SERS enhancement factors $(|E|/|E_0|)^4 \sim 10^4-10^5$ for Ag nanocubes.[62,63] If the *observable* electron emission current is assumed to originate predominantly from the top cube corners, the four-photon photoelectron emission cross-section is predicted to be $\sigma_{PE}^{(4)} = 5.2 \times 10^{-105}$ cm^8 s^3 for circularly polarized $\lambda = 800$ nm light based on the modified model of Yalunin et al. Circularly polarized light is employed in measuring the electron emission rate as a function of laser intensity to eliminate the signal dependence on the laser polarization direction. The calculated photoelectron emission cross-section compares rather well to the experimental results (see SI) that range from $\sigma_{PE}^{(4)} \sim 10^{-105}$ to 10^{-104} cm^8 s^3 for different Ag nanocubes. Note that the lower limit is likely to be another order of magnitude smaller (i.e., $\sigma_{PE}^{(4)} \sim 10^{-106}$ cm^8 s^3), because signals from many of the nanocubes (~40%) are found to be too small to distinguish from the support film background. Given the simplicity of our assumptions, experimental variations in the electron emissivity of different cubes, and semiquantitative evaluation of the electric near-field enhancement, the observed agreement is extremely good. We have previously shown that the same approach also predicts the observed electron emission rates in resonantly excited Au nanorods reasonably well.[25] This dual success in describing experimental photoelectron emission rates in two substantially different nanoparticle systems speaks substantially in support of such a coherent multiphoton model. In particular, the results indicate that: (i) coherent multiphoton photoelectron emission is likely a general phenomenon for metallic nanoparticles/nanostructures excited with ultrafast laser pulses with photon energy below material work function, and (ii) the role of nanoparticle plasmons can be effectively included into the coherent MPPE models by simple multiplication of the incident electric field by the near-field enhancement factor ($|E|/|E_0|$).

In an earlier study of two-photon photoelectron emission from small ($d = 3.6 \pm 0.8$ nm) Ag nanospheres, the alternative, *incoherent* MPPE process has been argued to yield ~10^3-fold lower photoelectron current than for a coherent process. Simply stated, this is because the energy (and momentum) of a decaying plasmon has to be transferred to an already excited electron among a much larger number of unexcited conduction electrons.[29] As the particle size and consequently the number of electrons (N_e) increases, the likelihood for such a process becomes progressively smaller, with the probability scaling as $P \sim (1/N_e)$. Additionally, involvement of three intermediate single-particle states in case of an incoherent four-photon ($n = 4$) photoelectron emission process would decrease the probability even further, $P \sim (1/N_e)^{n-1}$. Consequently, the role of incoherent MPPE is anticipated to be negligible compared to the coherent process, particularly as the number of involved photons, and thus intermediate states, increases.

The MPPE signal depends sensitively on the local electric field distribution $[(|E|/|E_0|)^8]$ and consequently all factors that affect the electric near-field. For example, local structure can dramatically influence the magnitude of the nanoparticle near-field, suggesting that the MPPE could in principle depend sensitively on tiny differences in topography of the particle surface. Indeed, these nanoparticle-to-nanoparticle variations in structure are likely responsible for observed asymmetries in the four-lobed images of MPPE rate versus excitation laser polarization (Figure 5a), where one diametrically opposed lobal pair is generally stronger than the other by typically 3- to 5-fold. However, for these fourth-order processes, such differences between the adjacent lobes would require only ≈22% (i.e., $5^{1/8} = 1.22$) variation in $|E|/|E_0|$ for neighboring cube corners, which would in turn be consistent with the slight topological imperfections observed in the HRTEM images.

Since curvature near the cube corners would appear a dominant structural factor influencing the local electric field enhancement, the inferred variation in $|E|/|E_0|$ within the same cube implies that the roundness of neighboring corners may slightly differ. Interestingly, we explored the link between observed photoelectron emission rates and the measured corner radii for $N = 8$ different cubes and found no clear correlation (see SI). This result is surprising and may suggest that only corner features smaller than a typical HRTEM resolution of ~1−2 nm significantly contribute to the overall photoemission signal. Alternatively, since the corner radius is not measured directly, but rather inferred from the roundness of the corresponding edges, the dominant topological sources contributing to the observed MPPE signal could simply have escaped observation. Indeed, the actual sharpness of the corner topology may be more readily identifiable in HRTEM by tilting the sample, as will be investigated in greater detail in the future.

In summary, spatial and polarization correlated DFM-HRTEM-SPIM studies of individual nanoparticles at high sensitivity and high signal-to-noise offer unique insight into the electron emission process following excitation with high-intensity ultrashort laser pulses. In particular, these studies identify coherent multiphoton photoelectron emission as the most probable mechanism responsible for electron emission from Ag nanocubes, and likely metal nanoparticles in general, when ultrafast excitation with photon energies smaller than the metal work function ($E_{ph} < \Phi$) is employed. The coherent

dx.doi.org/10.1021/nl302271u | Nano Lett. 2012, 12, 4823−4829

MPPE model proposed by Yalunin et al. predicts the experimentally measured absolute photoelectron emission rates reasonably well, with the simple modification that the incident electric field is augmented by the plasmon-induced electric near-field enhancement factor $|E|/|E_0|$.[39] According to the modified model, the photoelectron emission rate depends sensitively on $|E|/|E_0|$ by scaling approximately with $(|E|/|E_0|)^{2n}$, where n is the minimum number of photons required to overcome the material work function (i.e., $n > \Phi/E_{ph}$). For typical values of $n = 4$, the presence of a plasmon resonance can therefore dramatically enhance the total photoelectron emission yield, even for only relatively modest increase in the incident electric field near the particle surface. In a view toward future directions, this strong sensitivity of MPPE to the local electric field thus opens up the exciting possibility for quantitative "mapping" of plasmonic near-field enhancement factors in metallic nanoparticles and nanostructures in general.

■ ASSOCIATED CONTENT

Supporting Information

(i) Detailed methods and materials, (ii) distribution of cube sizes and dipolar plasmon resonance peaks, (iii) polarization dependence of the scattering signal observed for particles other than cubes, (iv) statistics on the polarization dependence of Ag nanocubes, (v) experimentally observed dependence of the electron emission rate of Ag nanocubes on the laser intensity and comparison with predictions of a coherent MPPE model as well as thermionic emission model with anomalous heating, and (vi) electron emission dependence on cube corner radius. This material is available free of charge via the Internet at http://pubs.acs.org.

■ AUTHOR INFORMATION

Corresponding Author

*E-mail: vanduyne@northwestern.edu and djn@jila.colorado.edu.

Author Contributions

⊥These authors contributed equally.

Notes

The authors declare no competing financial interest.

■ ACKNOWLEDGMENTS

A.G. and D.J.N. would like to thank the Air Force Office of Scientific Research for support of this work with additional funds for optics, microscopy, and computer resources provided by the National Science Foundation and the National Institute for Standards and Technology. E.R., L.D.M., and R.P.V.D. acknowledge support from the National Science Foundation (CHE-0911145) and the NSF MRSEC (DMR-1121262) at the Materials Research Center of Northwestern University. Y.X. was partially supported by the NSF (DMR-1104614).

■ REFERENCES

(1) Willets, K. A.; Van Duyne, R. P. *Annu. Rev. Phys. Chem.* **2007**, *58*, 267−297.
(2) Anker, J. N.; Hall, W. P.; Lyandres, O.; Shah, N. C.; Zhao, J.; Van Duyne, R. P. *Nat. Mater.* **2008**, *7* (6), 442−453.
(3) Sepúlveda, B.; Angelomé, P. C.; Lechuga, L. M.; Liz-Marzán, L. M. *Nano Today* **2009**, *4*, 244−251.
(4) Mayer, K. M.; Hafner, J. H. *Chem. Rev.* **2011**, *111*, 3828−3857.
(5) Zia, R.; Schuller, J. A.; Chandran, A.; Brongersma, M. L. *Mater. Today* **2006**, *9*, 20−27.
(6) Ozbay, E. *Science* **2006**, *311* (5758), 189−193.
(7) Aubry, A.; Lei, D. Y.; Fernández-Domínguez, A. I.; Sonnefraud, Y.; Maier, S. A.; Pendry, J. B. *Nano Lett.* **2010**, *10*, 2574−2579.
(8) Ebbesen, T. W.; Genet, C.; Bozhevolnyi, S. I. *Phys. Today* **2008**, *61*, 44−50.
(9) Hill, H. D.; Mirkin, C. A. *Nat. Protocols* **2006**, *1*, 324−336.
(10) Cobley, C. M.; Skrabalak, S. E.; Campbell, D. J.; Xia, Y. *Plasmonics* **2009**, *4*, 171−179.
(11) Stiles, P. L.; Dieringer, J. A.; Shah, N. C.; Van Duyne, R. P. *Ann. Rev. Anal. Chem.* **2008**, *1*, 601−626.
(12) Sharma, B.; Frontiera, R. R.; Henry, A.-I.; Ringe, E.; Van Duyne, R. P. *Mater. Today* **2012**, *15*, 16−25.
(13) Genevet, P.; Tetienne, J.-P.; Gatzogiannis, E.; Blanchard, R.; Kats, M. A.; Scully, M. O.; Capasso, F. *Nano Lett.* **2010**, *10*, 4880−4883.
(14) Chen, C. K.; Heinz, T. F.; Ricard, D.; Shen, Y. R. *Phys. Rev. B* **1983**, *27*, 1965−1978.
(15) Hulteen, J. C.; Young, M. A.; Van Duyne, R. P. *Langmuir* **2006**, *22*, 10354−10364.
(16) Milojevich, C. B.; Silverstein, D. W.; Jensen, L.; Camden, J. P. *J. Am. Chem. Soc.* **2011**, *133*, 14590−14592.
(17) Milojevich, C. B.; Silverstein, D. W.; Jensen, L.; Camden, J. P. *ChemPhysChem* **2011**, *12*, 101−103.
(18) Fort, E.; Grésillon, S. *J. Phys. D: Appl. Phys.* **2008**, *41*, 013001.
(19) Wustholz, K. L.; Henry, A.-I.; McMahon, J. M.; Freeman, R. G.; Valley, N.; Piotti, M. E.; Natan, M. J.; Schatz, G. C.; Van Duyne, R. P. *J. Am. Chem. Soc.* **2012**, *132*, 10903−10910.
(20) Giannini, V.; Fernández-Domínguez, A. I.; Heck, S. C.; Maier, S. A. *Chem. Rev.* **2011**, *111*, 3888−3912.
(21) Large, N.; Abb, M.; Aizpurua, J.; Muskens, O. L. *Nano Lett.* **2010**, *10*, 1741−1746.
(22) Kupersztych, J.; Monchicourt, P.; Raynaud, M. *Phys. Rev. Lett.* **2001**, *86* (22), 5180−5183.
(23) Polyushkin, D. K.; Hendry, E.; Stone, E. K.; Barnes, W. L. *Nano Lett.* **2011**, *11* (11), 4718−4724.
(24) Schweikhard, V.; Grubisic, A.; Baker, T. A.; Thomann, I.; Nesbitt, D. J. *ACS Nano* **2011**, *5* (5), 3724−3735.
(25) Grubisic, A.; Schweikhard, V.; Baker, T. A.; Nesbitt, D. J. submitted, **2012**.
(26) Hrelescu, C.; Sau, T. K.; Rogach, A. L.; Jackel, F.; Laurent, G.; Douillard, L.; Charra, F. *Nano Lett.* **2011**, *11* (2), 402−407.
(27) Evers, F.; Rakete, C.; Watanabe, K.; Menzel, D.; Freund, H. J. *Surf. Sci.* **2005**, *593* (1−3), 43−48.
(28) Gloskovskii, A.; Valdaitsev, D.; Nepijko, S. A.; Schonhense, G.; Rethfeld, B. *Surf. Sci.* **2007**, *601* (20), 4706−4713.
(29) Merschdorf, M.; Pfeiffer, W.; Thon, A.; Voll, S.; Gerber, G. *Appl. Phys. A: Mater. Sci. Process.* **2000**, *71* (5), 547−552.
(30) Rohmer, M.; Bauer, M.; Leissner, T.; Schneider, C.; Fischer, A.; Niedner-Schatteburg, G.; von Issendorff, B.; Aeschlimann, M. *Phys. Status Solidi B-Basic Solid State Phys.* **2010**, *247* (5), 1132−1138.
(31) Kubo, A.; Jung, Y. S.; Kim, H. K.; Petek, H. *J. Phys. B, At. Mol. Opt. Phys.* **2007**, *40* (11), S259−S272.
(32) Kubo, A.; Onda, K.; Petek, H.; Sun, Z. J.; Jung, Y. S.; Kim, H. K. *Nano Lett.* **2005**, *5* (6), 1123−1127.
(33) Fecher, G. H.; Schmidt, O.; Hwu, Y.; Schonhense, G. *J. Electron Spectrosc. Relat. Phenom.* **2002**, *126* (1−3), 77−87.
(34) Dushman, S. *Rev. Mod. Phys.* **1930**, *2* (4), 0381−0476.
(35) Richardson, O. W. *Emission of Electricity from Hot Bodies*; Longmans Green & Co.: London, 1921.
(36) Keldysh, L. V. *Sov. Phys. JETP-USSR* **1965**, *20* (5), 1307−&.
(37) Anisimov, S. I.; Benderskii, V. A.; Farkas, G. *Usp. Fiz. Nauk* **1977**, *122* (2), 185−222.
(38) Bechtel, J. H.; Smith, W. L.; Bloembergen, N. *Phys. Rev. B* **1977**, *15* (10), 4557−4563.
(39) Yalunin, S. V.; Gulde, M.; Ropers, C. *Phys. Rev. B* **2011**, *84* (19), 195426.
(40) Georges, A. T. *Phys. Rev. B* **1995**, *51* (19), 13735−13738.
(41) Skrabalak, S. E.; Au, L.; Li, X.; Xia, Y. *Nat. Protoc.* **2007**, *2*, 2182.
(42) Henry, A.-I.; Bingham, J. M.; Ringe, E.; Marks, L. D.; Schatz, G. C.; Van Duyne, R. P. *J. Phys. Chem. C* **2011**, *115*, 9291−9305.

(43) Ringe, E.; Zhang, J.; Langille, M. R.; Sohn, K.; Cobley, C. M.; Au, L.; Xia, Y.; Mirkin, C. A.; Huang, J.; Marks, L. D.; Van Duyne, R. P. *Mater. Res. Soc. Symp. Proc.* **2010**, *1208*, O10−02.
(44) Zhou, F.; Li, Z.-Y.; Liu, Y.; Xia, Y. *J. Phys. Chem. C* **2008**, *112* (51), 20233−20240.
(45) Monti, O. L. A.; Baker, T. A.; Nesbitt, D. J. *J. Chem. Phys.* **2006**, *125* (15), 154709.
(46) Schweikhard, V.; Grubisic, A.; Baker, T. A.; Nesbitt, D. J. *J. Phys. Chem. C* **2011**, *115* (1), 83−91.
(47) Bernath, P. F. *Spectra of Atoms and Molecules*; Oxford University Press: New York, 1995.
(48) Dweydari, A. W.; Mee, C. H. B. *Phys. Status Solidi A* **1973**, *17* (1), 247−250.
(49) Sherry, L. J.; Chang, S.-H.; Schatz, G. C.; Van Duyne, R. P.; Wiley, B. J.; Xia, Y. *Nano Lett.* **2005**, *5* (10), 2034−2038.
(50) McMahon, J. M.; Wang, Y.; Sherry, L. J.; Van Duyne, R. P.; Marks, L. D.; Gray, S. K.; Schatz, G. C. *J. Phys. Chem. C* **2009**, *113* (7), 2731−2735.
(51) Ringe, E.; McMahon, J. M.; Sohn, K.; Cobley, C. M.; Xia, Y.; Huang, J.; Schatz, G. C.; Marks, L. D.; Van Duyne, R. P. *J. Phys. Chem. C* **2010**, *114*, 12511−12516.
(52) McLellan, J. M.; Li, Z.-Y.; Siekkinen, A. R.; Xia, Y. *Nano Lett.* **2007**, *7*, 1013−1017.
(53) Pastoriza-Santos, I.; Sanchéz-Iglesias, A.; García de Abajo, F. J.; Liz-Marzán, L. M. *Adv. Funct. Mater.* **2007**, *17*, 1443−1450.
(54) Rodríguez-Fernández, J.; Novo, C.; Myroshnychenko, V.; Funston, A. M.; Sánchez-Iglesias, A.; Pastoriza-Santos, I.; Pérez-Juste, J.; García de Abajo, F. J.; Liz-Marzán, L. M.; Mulvaney, P. *J. Phys. Chem. C* **2009**, *113* (43), 18623−18631.
(55) Hu, M.; Chen, J.; Marquez, M.; Xia, Y.; Hartland, G. V. *J. Phys. Chem. C* **2007**, *111*, 12558−12565.
(56) Tcherniak, A.; Ha, J. W.; Dominguez-Medina, S.; Slaughter, L. S.; Link, S. *Nano Lett.* **2010**, *10*, 1398−1404.
(57) Munechika, K.; Smith, J. M.; Chen, Y.; Ginger, D. S. *J. Phys. Chem. C* **2007**, *111* (51), 18906−18911.
(58) Blaber, M. G.; Henry, A.-I.; Bingham, J. M.; Schatz, G. C.; Van Duyne, R. P. *J. Phys. Chem. C* **2012**, *116*, 393−403.
(59) Schubert, O.; Becker, J.; Carbone, L.; Khalavka, Y.; Provalska, T.; Zins, I.; Sönnichsen, C. *Nano Lett.* **2008**, *8*, 2345−2350.
(60) Johnson, P. B.; Christy, R. W. *Phys. Rev. B* **1972**, *6*, 4370−4379.
(61) Duan, H.; Fernández-Domínguez, A. I.; Bosman, M.; Maier, S. A.; Yang, J. K. W. *Nano Lett.* **2012**, *12*, 1683−1689.
(62) McLellan, J. M.; Siekkinen, A. R.; Chen, J.; Xia, Y. *Chem. Phys. Lett.* **2006**, *427*, 122−126.
(63) Rycenga, M.; Xia, X.; Moran, C. H.; Zhou, F.; Qin, D.; Li, Z.-Y.; Xia, Y. *Angew. Chem., Int. Ed.* **2011**, *50*, 5473−5477.